Fluorescent PNA Probes as Hybridization Labels for Biological RNA†

Kelly L. Robertson,‡,§ Liping Yu,‡,§ Bruce A. Armitage,*,‡ A. Javier Lopez,|| and Linda A. Peteanu*,‡

Department of Chemistry, Carnegie Mellon University, 4400 Fifth Avenue, Pittsburgh, Pennsylvania 15213-3890, and Department of Biological Sciences, Carnegie Mellon University, 4400 Fifth Avenue, Pittsburgh, Pennsylvania 15213-3890

Received October 8, 2005; Revised Manuscript Received March 17, 2006

ABSTRACT: Fluorescent labeling of biological RNA is complicated by the narrow range of nucleoside triphosphates that can be used for biological synthesis (i.e., transcription) as well as the inability to site-specifically incorporate them into long RNA transcripts. Noncovalent strategies for labeling RNA rely on attaching fluorescent dyes to hybridization probes which deliver the dye to a specific region of the RNA through Watson−Crick base pairing. This report demonstrates the use of high-affinity peptide nucleic acid (PNA) probes in labeling mRNA transcripts with thiazole orange donor and Alexa-594 acceptor fluorophores. The PNA probes were targeted to sequences flanking splice sites in a pre-mRNA such that before splicing the PNAs were separated by >300 nucleotides (nts) whereas after splicing the separation decreased to ≤12 nts. The decreased separation led to enhanced Förster resonance energy transfer (FRET) for the spliced RNA. Bulk solution and single-molecule fluorescence experiments gave consistent results.

RNA is a versatile biomolecule that is involved in many vital cellular processes. To fully understand its functions in the cell, it is necessary to directly monitor RNA conformational changes during events such as pre-mRNA splicing, ribosome assembly, and tRNA processing. While X-ray crystallography and NMR spectroscopy provide higher-resolution structural information, fluorescent labels allow sensitive probing of the structural dynamics and functions of RNA in real time and in solution (*1*−*3*).

RNA is not inherently fluorescent, so chemical methods are required to introduce fluorophores into RNA. Small RNA molecules (fewer than 60 bases) can be labeled through the incorporation of a fluorescent nucleotide analogue into solid-phase chemical synthesis or by postsynthetic attachment of a functionalized fluorophore to a modified base (*1*). Large RNA molecules are more difficult to label site-specifically because fluorescent nucleoside triphosphate analogues are randomly incorporated by RNA polymerase during transcription. This results in uniformly labeled RNA, analogous to radioactively labeled RNAs produced by transcription using a radioactive nucleoside triphosphate. Although uniform labeling allows for sensitive detection of the RNA, structural features cannot be probed since the fluorescent label is distributed throughout the molecule. Methods for 3′ and 5′ labeling have been reported (*1*, *4*) but restrict labeling to the RNA termini, which could be too far from sites of interest in the folded, functional RNA. Another labeling method which imposes fewer limitations on the modification site involves the use of T4 DNA ligase along with a DNA oligonucleotide splint (*5*). This method allows the RNA to be synthesized and labeled in pieces, which can then be ligated to form the full-length RNA. However, problems associated with this technique such as interference with DNA hybridization by RNA secondary structure and low ligation yields have limited its usefulness (*1*). An interesting variation on this method was introduced recently and utilizes an engineered "twin ribozyme" that first excises a small region of a RNA and then replaces it with a small modified RNA fragment (*6*). This method was shown to be most successful if the modified RNA fragment has a more stable interaction with the ribozyme than the natural RNA fragment, and therefore, changes in sequence of the modified fragment may be necessary to improve the efficiency of the reaction. Also, as with the previous method, RNA secondary and tertiary structure may interfere with the binding of the ribozyme and thus decrease the product yield.

Several recent reports have demonstrated the potential for noncovalent labeling methods using fluorescent hybridization probes. By utilizing Watson−Crick base pairing rules, hybridization probes can theoretically be used to introduce noncovalent labels anywhere within a RNA molecule, although again competition from RNA secondary and tertiary structure can block access to certain regions. Much work has been done on the use of hybridization probes for the labeling of nucleic acids (*7*−*13*). In several cases, cohybridization of two probes labeled with donor and acceptor fluorophores allowed the use of Förster resonance energy transfer (FRET)[1] in the study of structural dynamics. FRET is a nonradiative process in which energy is transferred from a donor fluorophore to an acceptor fluorophore in a distance-

† This research was supported by a seed grant from the Interdisciplinary Research Fund (Carnegie Mellon University), and L.A.P. acknowledges support from a special creativity extension to NSF Grant CHE-0109761.

* To whom correspondence should be addressed. L.A.P.: telephone, (412) 268-1327; fax, (412) 268-6897; e-mail, peteanu@andrew.cmu.edu. B.A.A.: telephone, (412) 268-4196; fax, (412) 268-1061; e-mail, army@andrew.cmu.edu.

‡ Department of Chemistry.

§ These authors contributed equally to the research reported here.

|| Department of Biological Sciences.

[1] Abbreviations: FRET, Förster resonance energy transfer; TO, thiazole orange; PNA, peptide nucleic acid; TIRF, total internal reflection fluorescence.

10.1021/bi052050s CCC: $33.50 © 2006 American Chemical Society
Published on Web 04/22/2006

dependent manner (*14*). The combination of hybridization probes and FRET has been used successfully for the detection of specific mRNA sequences both in vitro and in vivo (*9*−*11*). In addition, it was shown that hybridization probes can be used to site-specifically label engineered hairpin extensions in both the ribosome (*12*) and the RNase P ribozyme (*13*).

DNA-based probes can be modified easily and cost-effectively with various fluorophores and labels, but they suffer from two important limitations. First, the main challenge of using any hybridization probe is competition from local secondary and tertiary structure in the RNA. The relatively low affinity of DNA for complementary RNA requires that either long DNA probes be used or effective target sites be limited to unstructured regions of the RNA. In some cases, unnatural "extensions" have to be added to loop regions of a target RNA to allow DNA hybridization probes to bind (*12*, *13*). The second disadvantage to DNA probes is that successful hybridization yields a DNA−RNA duplex that could be a substrate for RNase H. Thus, these probes could stimulate degradation of the target rather than simply reporting on its presence and structure, depending on the conditions under which experiments are performed.

One way to address both the probe length and RNase H activation limitations of DNA hybridization probes is to use unnatural, high-affinity analogues of DNA. This report focuses on one of these analogues, peptide nucleic acid (PNA) (*15*, *16*). PNA has the same hydrogen bonding nucleobases as DNA, but they are attached to an uncharged pseudopeptide backbone. The lack of electrostatic repulsion allows PNA to hybridize strongly to complementary RNA (*17*). Because PNA forms highly stable duplexes with RNA, the length of the hybridization probe can be decreased substantially, relative to the length of the analogous DNA probe. In addition, RNase H fails to recognize the unnatural structure of a PNA−RNA duplex (*18*, *19*). While this is a deficiency for using PNA as an antisense agent, it is a benefit for labeling applications. Previously, a donor PNA hybridization probe was used along with an acceptor DNA hybridization probe in a FRET-based system to allow the precise quantification of the mutant genotype in fibrous dysplasia/McCune-Albright syndrome (*20*).

The work described here presents a method that utilizes fluorescent PNA hybridization probes to site-specifically label large RNA transcripts. Using PNA labeled with the fluorogenic dye thiazole orange, we are able to show that fluorescent PNA probes can bind to a large RNA target and produce changes in fluorescence that correspond to hybridization events. Furthermore, two probes fluorescently labeled to undergo FRET can hybridize to areas flanking the splice sites of a mRNA molecule and demonstrate a difference in FRET efficiency between spliced and unspliced mRNA, as shown by both bulk solution and single-molecule spectroscopy measurements. The results demonstrate that such probes should be suitable for measurements of the kinetics of RNA processing reactions as well as dynamical measurements of RNA structural fluctuations using single-molecule methods (*21*).

EXPERIMENTAL PROCEDURES

Materials. All DNA oligonucleotides were purchased from Integrated DNA Technologies, Inc., as lyophilized powders which were purified by gel filtration chromatography. The RPS14A pre-mRNA and mRNA were prepared in the Lopez lab by in vitro transcription from genomic DNA and cDNA templates, respectively, into which promoters for T7 RNA polymerase were introduced by polymerase chain reaction amplification; the RNAs were purified by gel electrophoresis. Boc/Z-protected PNA monomers were purchased from Applied Biosystems (Foster City, CA). Boc-protected lysine and Boc-protected glutamic acid were purchased from Nova Biochem (San Diego, CA). *p*-Methyl benzylhydramine·HCl (MBHA) 0.17 mequiv/g loading resin was purchased from Peptide International (Louisville, KY). The succinimidyl ester-derivatized AlexaFluor-594 fluorophore was purchased from Molecular Probes (Eugene, OR). The carboxylic acid derivative of thiazole orange (TO) dye was synthesized according to the literature method (*22*, *23*).

Chart 1: PNA Oligomers Used in This Study with Their Calculated and Observed Masses

Name	*Mass (calc.)*	*Mass (obs.)*
P1-10	2904.9	2905.2
P1-10$_A$	3612.8	3611.5
P1-10$_{TO}$	3293.3	3294.5
P1-13	3706.8	3706.7
P1-13$_A$	4414.6	4415.3
P2-10	2881.8	2882.2
P2-10$_{TO}$	3397.3	3396.1
P2-13$_{TO}$	4199.1	4198.4

PNA oligomers were synthesized using standard solid-phase peptide synthesis methods (*24*, *25*) and purified using reversed-phase high-performance liquid chromatography (RP-HPLC). PNAs were characterized by matrix-assisted laser desorption ionization time-of-flight (MALDI-TOF) mass spectrometry using α-cyano-4-hydroxycinnamic acid as the matrix (Chart 1). Synthesis of the N-terminally labeled PNA probes was performed on a 100 mg scale using either Boc-protected Glu-MBHA resin (**P1**−**10$_A$** and **P1**−**13$_A$**) or Boc-protected Lys-MBHA resin (**P1**−**10$_{TO}$**). (The C-terminal glutamic acid residue was used in place of lysine to allow selective conjugation of the Alexa dye to the N-terminus of PNA without interference from the lysine side chain.) **P1**−**10$_A$** and **P1**−**13$_A$** were cleaved and purified before labeling with Alexa-594 according to the manufacturer's protocol.

P1−**10$_{TO}$** was labeled with the carboxylic acid derivative of thiazole orange at its N-terminus prior to cleavage by following the same procedure for coupling PNA monomers. Synthesis of the C-terminally labeled probes was performed on a 75 mg scale using thiazole orange-labeled Boc-protected Lys-MBHA resin. The thiazole orange-labeled resin was synthesized by reacting 500 μL of 0.4 M thiazole orange carboxylic acid derivative with 500 μL of 0.4 M Boc-Lys-OH using 500 μL of 0.8 M DIEA and 1000 μL of 0.38 M HATU as coupling agents (all solutions were prepared in NMP). The product TO-Boc-Lys was purified by reversed-phase HPLC and analyzed by ESI/APCl-ion trap-MS (*m*/*z* calcd 633.8, *m*/*z* observed 633.1). Upon drying, the entire product (approximately 25 mg) was used for attachment to MBHA resin. The TO-Boc-Lys was dissolved in 150 μL of NMP and mixed with 150 μL of 0.5 M DIEA, 180 μL of 0.2 M HATU, and 1.3 mL of NMP. The solution was

allowed to activate for 2 min before being added to 150 mg of MBHA resin and incubation at room temperature overnight. The TO-Lys-loaded resin was dried and used to synthesize the **P2**−**10$_{TO}$** and **P2**−**13$_{TO}$** probes by standard automated solid-phase peptide synthesis. PNA stock solutions were prepared in water, and concentrations were determined at 260 nm and 85 °C. Extinction coefficients for PNA monomers were obtained from PE Biosystems (C = 6600 M^{-1} cm^{-1}; T = 8600 M^{-1} cm^{-1}; A = 13 700 M^{-1} cm^{-1}; G = 11 700 M^{-1} cm^{-1}).

Thermal Analysis. Thermal analyses were performed on a Varian Cary 3 Bio UV−vis spectrophotometer equipped with a thermoelectrically controlled multicell holder. The samples were prepared in a buffer containing 100 mM NaCl, 10 mM sodium citrate (pH 6.4), and 0.1 mM EDTA. Samples were heated to 90 °C and equilibrated for 5 min. Absorbance measurements at 275 nm were recorded every 1 °C as samples were cooled and then heated at 1.0 °C/min.

Hybridization to RNA Targets. Bulk solution fluorescence experiments were performed on either a PTI spectrofluorometer or a SPEX FluoroMax-2 spectrofluorometer. All samples contained 25 nM **P1**−**10$_{TO}$** or **P2**−**10$_{TO}$** alone or with 25 nM spliced or unspliced RNA. Samples were annealed in buffer containing 100 mM NaCl, 10 mM sodium citrate (pH 6.4), and 0.1 mM EDTA, and emission spectra were recorded from 500 to 700 nm with excitation at 490 nm.

Fluorescence Emission Quantum Yield Measurements. The quantum yields of the TO- and Alexa-conjugated PNA probes were measured while hybridized to **D32** using as the standard rhodamine 6G in pure ethanol (quantum yield of 0.95) (*26*). Each probe was hybridized to 32mer DNA in a buffer containing 10 mM sodium phosphate and 100 mM NaCl (pH 7) in a series of concentrations (200, 400, 600, and 800 nM) chosen such that the absorption did not exceed 0.1 (*27*). Absorbance and fluorescence spectra of the series of samples were recorded. A graph of integrated fluorescence intensity versus absorption was plotted, and the quantum yield was calculated according to the following equation (*28*)

$$\Phi_X = \Phi_{ST}\left(\frac{Grad_X}{Grad_{ST}}\right)\left(\frac{\eta_X^2}{\eta_{ST}^2}\right)$$

where the subscripts ST and X represent standard and test sample, respectively, Φ is the fluorescence quantum yield, Grad is the gradient from the plot of integrated fluorescence intensity versus absorption, and η is the refractive index of the solvent.

Bulk Fluorescence Resonance Energy Transfer (FRET) Measurements. Samples were prepared in buffer containing 100 mM NaCl, 10 mM sodium citrate (pH 6.4), and 0.1 mM EDTA. Emission spectra were measured from 500 to 700 nm with excitation at 480 nm. All spectra were recorded at 25 °C with a 5 nm band-pass on both the excitation and emission monochromators. The FRET efficiencies of the four probe pairs were calculated while they were hybridized to the spliced RNA, unspliced RNA, and 32mer DNA model by measuring the fluorescence of (a) the donor probe (**P2**−**10$_{TO}$** or **P2**−**13$_{TO}$**), (b) the acceptor probe (**P1**−**10$_{A}$** or **P1**−**13$_{A}$**), and (c) the donor and acceptor probes. In the cases of the donor only and acceptor only measurements, equimolar amounts of unlabeled probes (acceptor and donor, respectively) were included. For example, in Figure 4, samples containing (i) **P2**−**10$_{TO}$** and **P1**−**10**, (ii) **P1**−**10$_{A}$** and **P2**−**10**, or (iii) **P1**−**10$_{A}$** and **P2**−**10$_{TO}$** were annealed to spliced RNA. Spliced and unspliced RNA solutions contained all species at 2 nM, and 32mer DNA solutions contained all species at 25 nM. Three scans were recorded and averaged for all cases. The donor plus acceptor spectra were corrected for the direct excitation of Alexa-594 by subtracting the acceptor only spectra for all probe pairs. The efficiency of energy transfer was then calculated using the quenching of the donor in the presence of the acceptor by using eq 1:

$$E = 1 - I_{DA}/I_D \quad (1)$$

where I_{DA} and I_D are the donor intensities in the presence and absence of the acceptor, respectively.

Single-Molecule FRET Measurements. Samples of the PNA−DNA and PNA−RNA hybrids at 1 nM to which a 1% (v/v) oxygen scavenging solution [0.1 mg/mL glucose oxidase, 0.02 mg/mL catalase, 1% β-mercaptoethanol 3% (w/w) glucose, and 10 mM $MgCl_2$ (*29*)] was added were immobilized for study onto a streptavidin-coated microscope slide which was fitted with a sealable flow channel to allow the introduction of reagents. The slide was prepared by successive additions of 30 μL of 1 mg/mL biotinylated BSA (Sigma) in 10 mM Tris buffer (pH 8) and 30 μL of 0.2 mg/mL streptavidin (Molecular Probes) in 10 mM Tris buffer, incubation for 10 min, and washing with 10 mM Tris buffer. For experiments with **D32**, the DNA strand was modified with a 3′-biotin group to allow immobilization on the streptavidin-coated slide. For RNA experiments, a biotinylated DNA capture probe (5′-biotin-GACGTATGAGCTGAT-3′) complementary to the 3′-end of the RNA was used to immobilize the RNA on the slide. This strand was annealed to the RNA at the same time as the fluorescent PNA probes before immobilization.

The single-molecule experiments of labeled DNA were performed using both total internal reflection (TIR) illumination and confocal illumination, both of which gave similar results within our error. The experiments on labeled RNA were performed using scanning confocal fluorescence microscopy alone. Through objective TIR illumination was achieved using an inverted fluorescence microscope (Olympus IX-71) outfitted with a 60 × 1.4 NA oil immersion objective (Olympus) and a CCD camera (Coolsnap, Roper Scientific). Images of the donor and acceptor channels were obtained by rapidly switching between band-pass filters appropriate for the donor and acceptor channels (D540/50 for TO and D630/60 for Alexa-594, both from Chroma) placed in front of the camera. The image exposure times were 1 s. Data acquisition and analysis were performed using Image-Pro (Phase 3 Imaging Systems). FRET histograms were developed by measuring the emission intensity of each molecule in the field of view in both the donor and acceptor channels. In a separate experiment in which 1 s exposure times were used for a total measurement time of ∼20 s for each field of view that was examined, it was determined that little or no decrease in the emission intensity of either dye occurred over this time frame under the excitation conditions that were used. Each histogram represents the average of the results from ∼300 molecules examined in 10−20

separate fields of view in a total of two to three independent studies.

Scanning confocal measurements of the same molecular systems were performed on a home-built system consisting of the same microscope and objective used in the TIRF experiments but with the addition of an ultrathin piezoelectric scanning stage (Nanonics, NIS-70). The fluorescence passes through a dichroic beam splitter (Chroma, 585DCXR) which splits the emission of TO from that of Alexa and directs it to two avalanche photodiodes (APDs, Perkin-Elmer, single-photon counting module SPCM-AQR14) that sit at 90° to one another. The band-pass filter for TO is placed in front of the APD at the donor channel, and the one for Alexa is placed in front of the other APD to minimize cross talk. Integration times of 5 ms were used for APDs to read the photon counts, and 20 μm × 20 μm areas were scanned on the sample slides. The emissions of the two dyes were detected at the same time, and the corresponding scanned images were plotted simultaneously. The intensity on each molecule was read in a program written in Labview (National Instruments), and the background intensity was subtracted for calculations. Histograms of the data were then constructed.

For the TIRF experiments, the 476 nm line of an argon ion laser was used for excitation with the power at the input port of the microscope set at 600 μW. In the confocal experiments, the 488 nm line of an argon ion laser was used for excitation with the power at the input port of the microscope set at 20 μW. The cross talk from the donor emission into the acceptor channel was quantified for both excitation conditions by measuring the emission of a construct containing only the TO probe hybridized to DNA, mRNA, or pre-mRNA. It was found to be 25% for 476 nm excitation and 40% for 488 nm excitation and was a part of the FRET efficiency calculations. No correction for direct excitation of the acceptor molecules by either 476 or 488 nm light was made as experiments using constructs containing the acceptor alone determined that this contribution is negligible ($\leq$5%).

RESULTS

The goal of this study was to demonstrate that relatively short PNA probes could be used for fluorescent labeling of biologically interesting regions of a large RNA target. PNA probes with two different lengths (10 or 13 bases) and with two different attached fluorophores (thiazole orange or Alexa-594) were synthesized by standard methods (*24*, *25*). PNA sequences and fluorescent label structures are shown in Chart 2.

Hybridization to DNA Oligomers. PNA oligomers typically hybridize to complementary DNA and RNA targets with high affinity, yielding base-paired duplexes with high thermal stabilities (*17*). UV melting curves were recorded for the unmodified 10mer PNA probes and their respective complementary DNA 10mers (Chart 2 and Figure 1). Stable duplexes are formed in both cases, with T_m values of 73 and 54 °C for **P1**−**10**/**D1** and **P2**−**10**/**D2**, respectively. The higher T_m for **P1**−**10**/**D1** can be attributed to the higher G-C content of this duplex as well as the presence of three consecutive guanines on the PNA strand, which is known to give anomalously high thermal stabilities in PNA−DNA duplexes (*30*).

Characterization of the TO-Alexa-594 FRET Pair in a DNA Model System. A 32-nucleotide DNA strand (**D32**) was used as a model for the spliced mRNA target to be probed in later experiments to characterize the fluorescence properties of dye-conjugated PNA probes. Alexa-594-labeled probes **P1**−$\mathbf{13_A}$ and **P1**−$\mathbf{10_A}$ are complementary to the 5′-terminal 13 or 10 nucleotides of **D32**, while TO-labeled probes **P2**−$\mathbf{13_{TO}}$ and **P2**−$\mathbf{10_{TO}}$ are complementary to the 3′-terminal 13 or 10 nucleotides. On the basis of the calculated overlap between the TO emission and Alexa-594 absorption spectra, hybridization of TO- and Alexa-labeled probes at opposite ends of the DNA should permit FRET to occur with a critical transfer (Förster) distance, R_0, of 21 ± 1 Å. By placing the TO donor at the C-terminal position of the **P2** probes and the Alexa acceptor at the N-terminal position of the **P1** probes, we will position the fluorophores internally since PNA preferentially hybridizes by orienting its C-terminus with the 5′-terminus of DNA or RNA (*17*). (Scheme 1 shows the case for hybridization of **P1**−$\mathbf{10_A}$ and **P2**−$\mathbf{10_{TO}}$ to **D32**.) The fluorophores will be separated by 6, 9, or 12 nucleotides (minus the length of the linkers connecting the dyes to the PNAs) depending on which probe combination is used.

The quantum yields of the TO- and Alexa-conjugated PNA probes were measured while hybridized to **D32** using as the standard rhodamine 6G in pure ethanol. The quantum yields of the TO PNA−DNA constructs were found to depend weakly on the length of the PNA strands. When the 13mer PNA strand (**P2**−$\mathbf{13_{TO}}$) is hybridized to **D32**, the quantum yield is 0.15 ± 0.03, while that for TO on the 10mer strand (**P2**−$\mathbf{10_{TO}}$) is found to be 0.10 ± 0.03. These values are similar to the quantum yield measured for the nonconjugated thiazole orange monocation intercalated into double-helical DNA (*31*). Note that TO is nonfluorescent when free in solution due to rapid nonradiative decay. However, restriction of the conformational mobility in a viscous solvent or by intercalation into DNA results in a large increase in fluorescence (*32*). It is possible that the PNA-conjugated dye folds back and binds to the PNA−DNA duplex, but this is unlikely because intercalating dyes in general have a low affinity for PNA−DNA duplexes (*33*). Thus, when the TO-labeled PNA hybridizes to **D32**, the dye likely stacks either on the end of the PNA−DNA hybrid or between unpaired bases beyond the duplex region (*23*). The weak strand length dependence of quantum yields of the TO−PNA−DNA constructs is likely to be due to small changes in their TO stacking geometries or to specific interactions with the bases at the end of the PNA−DNA duplex. In contrast, Alexa-594−PNA−DNA constructs (**P1**−$\mathbf{13_A}$ and **P1**−$\mathbf{10_A}$) were found to have the same quantum yield (0.90 ± 0.04) irrespective of PNA strand length.

To estimate the Förster distance for this dye pair, different combinations of TO− and Alexa−PNA strands hybridized to **D32** were prepared having distances between the donor and acceptor of 6, 9, or 12 nucleotides. The FRET efficiency of these constructs was determined by comparing the TO donor fluorescence intensity in the presence of the Alexa-labeled PNA with the corresponding intensity when an unlabeled version (i.e., **P1**−**10** or **P1**−**13**) was cohybridized with **D32**. Data obtained at the single-molecule level and in bulk solution gave consistent results (Figure 2). The Förster

Chart 2: PNA Probes and Fluorescent Dyes Used in This Study[a]

Probe	Sequence
P1-10	H_2N-Glu-CTTGGGCGGT-H
P1-10$_A$	H_2N-Glu-CTTGGGCGGT-***A***
P1-10$_{TO}$	H_2N-Glu-CTTGGGCGGT-***TO***
P1-13	H_2N-Glu-CTTGGGCGGTACA-H
P1-13$_A$	H_2N-Glu-CTTGGGCGGTACA-***A***
P2-10	H_2N-Lys-CGAGCTTGAA-H
P2-10$_{TO}$	H_2N-***TO***(Lys)-CGAGCTTGAA-Lys-H
P2-13$_{TO}$	H_2N-Lys-CGAGCTTGAAACA-***TO***
D1	5'-GAACCCGCCA-3'
D2	5'-GCTCGAACTT-3'
D32	5'-GAACCCGCCATGTCTAACGTTGTT CAAGCTCG-Biotin-3'*

* Biotin was needed for single molecule experiments. See Methods section for details.

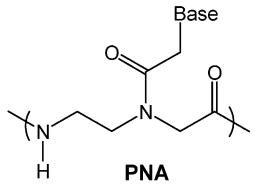

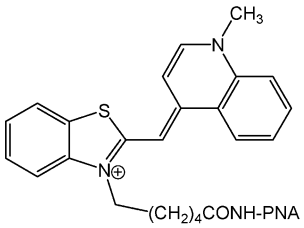

***N*-Terminal TO**

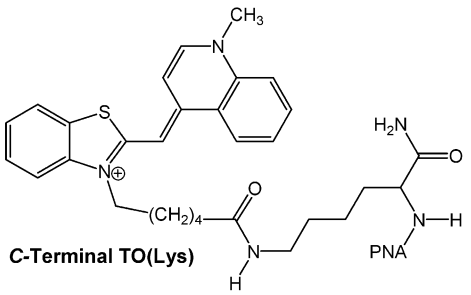

***C*-Terminal TO(Lys)**

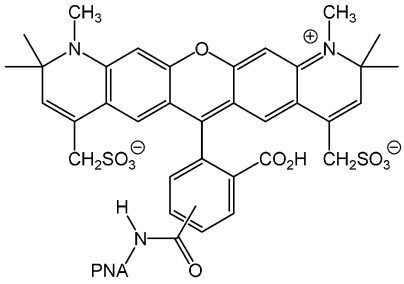

***N*-Terminal Alexa**

[a] ***TO*** is thiazole orange, and ***A*** is Alexa-594. Biotin was needed for single-molecule experiments. See Materials and Methods for details.

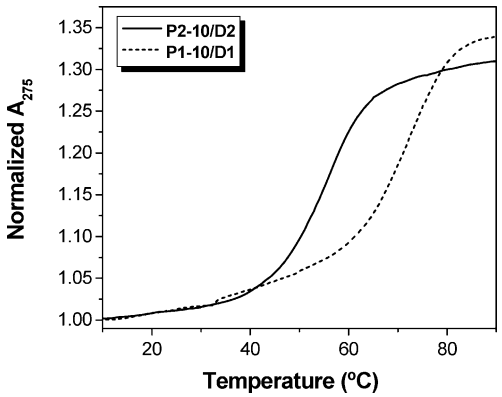

FIGURE 1: UV melting curves recorded for PNA probes **P1**−**10** and **P2**−**10** hybridized to their respective DNA complementary strands. [PNA] = [DNA] = 2.0 μM. The absorbance at 275 nm was normalized to the lowest temperature value.

distance estimated by this method is ~7 nt (Figure 2) or ~24 Å.

Scheme 1 [a]

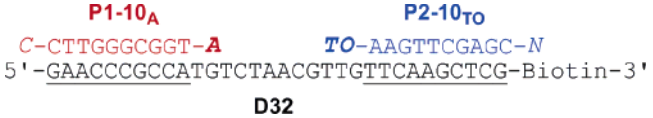

D32

[a] The C-terminus of **P1**−**10$_A$** and the N-terminus of **P2**−**10$_{TO}$** are shown.

Hybridization to RNA Targets. The results presented above illustrate distance-dependent FRET between TO- and Alexa-594-labeled PNAs hybridized to a DNA 32mer. We next evaluated hybridization to longer targets, specifically spliced and unspliced messenger RNA from the *RPS14A* gene that encodes the 40S ribosomal subunit protein rps14 in yeast. The target sites in the RNAs were (a) upstream of the 5′-splice site and (b) downstream of the 3′-splice site (Scheme 2) and were chosen for two reasons. First, there should be relatively little competing secondary structure in the vicinity of the splice sites. Second, probes hybridized to the two target sites should be much closer in the spliced RNA, allowing

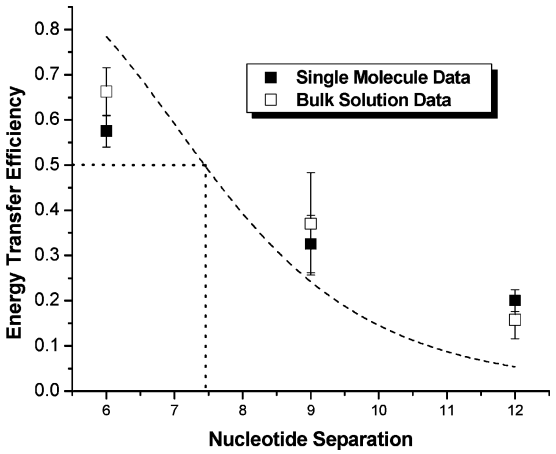

FIGURE 2: Summary of the single-molecule and bulk FRET results for the TO/Alexa-594−PNA−DNA constructs. The data for constructs having a 9 nt separation have larger error bars because there are two probe combinations (**P2**−$\mathbf{10_{TO}}$/**P1**−$\mathbf{13_A}$ and **P2**−$\mathbf{13_{TO}}$/**P1**−$\mathbf{10_A}$) with this separation that each gave slightly different FRET efficiencies. The dashed curve shows the results of a Förster calculation (see the text).

Scheme 2

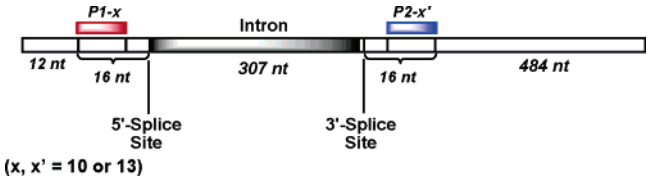

FRET to occur with greater efficiency than in the unspliced RNA. The 10mer probes described in the previous section hybridize to within six nucleotides of the splice sites, so they will be 330 nts apart in the unspliced RNA but only 12 nts apart in the spliced RNA. The target sites for the 13mer probes extend three nucleotides closer to the splice sites, so the FRET efficiency for the spliced form should be greater than with the 10mer probes.

Hybridization of PNA or any other short oligomer to a much larger target nucleic acid is not readily monitored by traditional methods such as UV melting curves or circular dichroism spectropolarimetry due to the high background absorbance contributed by the target alone. Similarly, electrophoretic mobility shifts in gels can be difficult to detect if hybridization of the probe does not substantially alter the mass:charge ratio. Fluorogenic labels offer an alternative method that allows detection of hybridization in solution and at low nanomolar concentrations (*34*). One such label is the thiazole orange dye described in the previous section. This dye was originally developed as a DNA stain (*33*) but was recently conjugated to PNA oligomers to produce "light-up" probes (*23*, *35*−*38*). TO-labeled PNA probes exhibit significant increases in fluorescence upon hybridization to DNA and RNA targets due to restricted conformational freedom in the fluorophore.

Figure 3 shows fluorescence spectra recorded for **P1**−$\mathbf{10_{TO}}$ free in solution and when bound to either the spliced or unspliced *RPS14A* RNA. There is significant fluorescence from the PNA probe even in the absence of the RNA target, an effect that has been attributed to association of the TO label with the PNA bases (*39*). However, when the RNA is present, the fluorescence of the PNA increases 3.5-fold. A

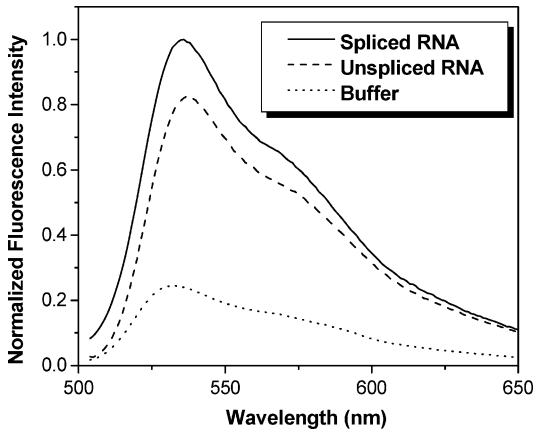

FIGURE 3: Fluorescence spectra recorded for **P1**−$\mathbf{10_{TO}}$ in buffer (•••) and in the presence of either unspliced (- - -) or spliced (—) RNA. [PNA] = [RNA] = 10 nM. Samples were excited at 490 nm.

Table 1: Fluorescence Enhancements[a] for Thiazole Orange (TO)-Labeled PNA Probes When Hybridized to RNA Targets

PNA	unspliced RNA	spliced RNA
P1−$\mathbf{10_{TO}}$	3.5	4.5
P2−$\mathbf{10_{TO}}$	1.9	2.5

[a] Enhancements are relative to the TO-labeled PNA alone.

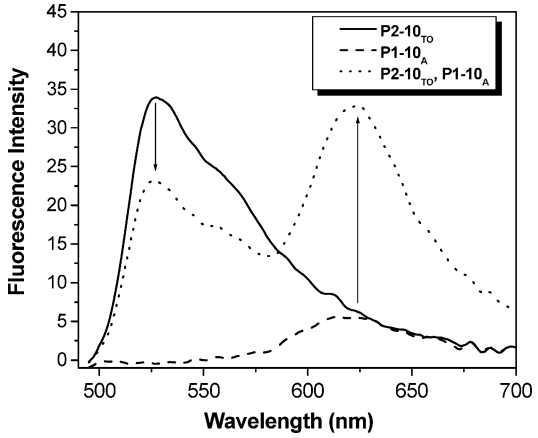

FIGURE 4: Fluorescence spectra recorded for spliced *RPS14A* mRNA labeled with **P1**−$\mathbf{10_{TO}}$ (—), **P2**−$\mathbf{10_A}$ (- - -), or both probes (•••). The arrows indicate quenching of the TO donor fluorescence and sensitized Alexa-594 acceptor fluorescence due to FRET. [RNA] = [PNA] = 25 nM. Samples were excited at 480 nm.

similar fluorescence enhancement is seen for binding of **P1**−$\mathbf{10_{TO}}$ to the spliced version of the RNA (Table 1). Furthermore, when the TO label is attached to the C-terminus of **P2**−**10** (**P2**−$\mathbf{10_{TO}}$), fluorescence is enhanced upon binding to both RNA targets (Table 1). The weaker enhancements for **P2**−$\mathbf{10_{TO}}$ are due to greater fluorescence of the probe in the absence of RNA rather than weaker fluorescence in the presence of RNA (data not shown). Regardless of the quantitative differences between the probes, the TO label allows PNA hybridization to RNA targets hundreds of nucleotides long to be easily detected in solution at low nanomolar concentrations.

FRET between Hybridized Probes. Figure 4 contains fluorescence spectra recorded from solutions containing (a) **P2**−$\mathbf{10_{TO}}$ alone, (b) **P1**−$\mathbf{10_A}$ alone, and (c) both PNAs together in the presence of spliced RNA. The energy transfer efficiency can be estimated on the basis of the quenching of

Table 2: FRET Efficiencies for PNA Probes Hybridized to RNA Targets

PNA probes[a]	unspliced RNA[b]	spliced RNA[b]	unspliced RNA[c]	spliced RNA[c]
P1−10$_A$ (12) **P2−10$_{TO}$**	0.14 ± 0.03	0.29 ± 0.04	0.12 ± 0.06	0.35 ± 0.02
P1−13$_A$ (9) **P2−10$_{TO}$**	0.13 ± 0.07	0.61 ± 0.06	0.10 ± 0.08	0.45 ± 0.05
P1−10$_A$ (9) **P2−13$_{TO}$**	0.51 ± 0.11	0.76 ± 0.03	0.42 ± 0.05	0.58 ± 0.06
P1−13$_A$ (6) **P2−13$_{TO}$**	0.05 ± 0.08	0.78 ± 0.04	0.07 ± 0.03	0.70 ± 0.04

[a] The number in parentheses corresponds to number of nucleotides separating the probes. [b] From bulk solution measurements. [c] From single-molecule measurements. Standard deviations for the single-molecule results represent the deviations of the mean of several measured distributions rather than the width of any given distribution.

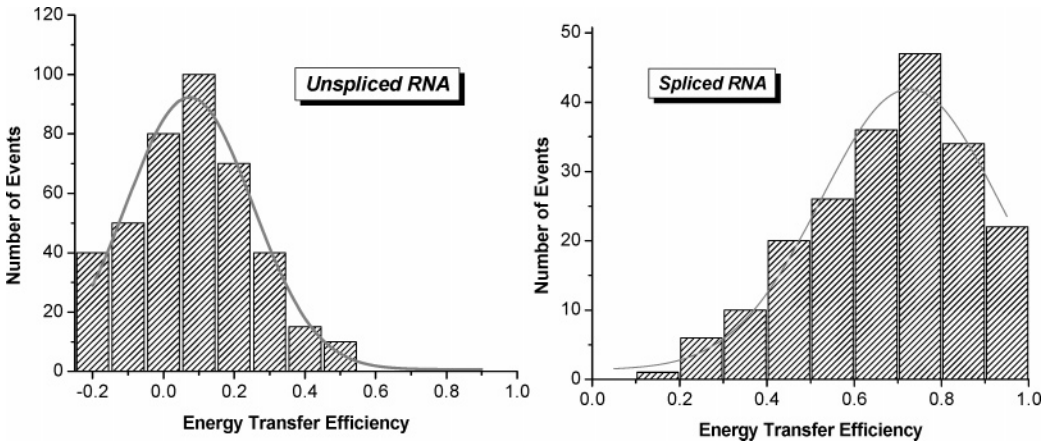

FIGURE 5: Single-molecule FRET results for **P2−13$_{TO}$**/**P1−13$_A$**-labeled pre-mRNA (left) and spliced mRNA (right). The smooth gray lines show the Gaussian fit to the histograms that contain the results from ~300 molecules. Note that the negative FRET values are due to subtraction of the cross talk from the donor to the acceptor channels.

the TO probe fluorescence in the presence of the Alexa-labeled probe. For the spliced RNA, this quenching corresponds to 29%, while for the unspliced RNA, only 14% quenching is observed (data not shown). This is consistent with the fact that the probes should be closer to one another on average in the spliced RNA than in the unspliced RNA. Table 2 contains the FRET efficiencies determined in this manner for four different probe combinations. For the spliced RNA, the FRET efficiency increases as the distance between the labels decreases, as expected. The efficiencies for the unspliced RNA are low, with the exception of the combination of **P1−10$_A$** and **P2−13$_{TO}$** (51%). While the reason for this anomalously high value is unknown, the FRET efficiency increases for the spliced RNA, as expected.

Single-molecule studies of the same constructs yielded values similar to the bulk measurements (Table 2), including that for the anomalous probe combination (**P1−10$_A$** and **P2−13$_{TO}$**). Sample distributions for the pre- and postsplicing RNA constructs are shown in Figure 5. The width of the RNA distributions shown, which likely reflects RNA conformational heterogeneity, is similar to those measured for the model PNA−DNA constructs (data not shown).

DISCUSSION

Recognition of the numerous roles played within the cell by RNA is creating a demand for better methods for detecting and probing the structure and function of biological RNAs. The cost of chemically synthesized RNA as well as limitations on biosynthesizing RNA site-specifically modified with fluorescent labels hinders progress in this area. An approach taken by several reports involves using a synthetic DNA oligomer (or DNA analogue) with a covalently attached fluorophore to hybridize with a complementary sequence in the RNA of interest, thereby delivering the fluorescent label to the intended site (*6*−*12*). We have followed the same strategy, but using PNA to deliver the fluorophore. The high affinity of PNA for RNA, the ease with which PNA can be synthesized with various fluorescent labels, and the inability of RNase H to recognize PNA−RNA hybrids make this an attractive candidate for RNA labeling.

The results presented above clearly demonstrate the utility of PNA probes for labeling biological RNAs such as the unspliced and spliced versions of the *RPS14A* mRNA. While our results cannot be compared with those of other studies using DNA-based fluorescent hybridization probes, in general, the high affinity of PNA will allow (i) shorter probes to be used and (ii) hybridization to more structured regions of the RNA. In cases where there is concern about a hybridization probe interfering with the biological function of the RNA, helical extensions have been introduced into surface accessible regions of the RNA and have been successfully targeted by hybridization probes (*12*). PNA probes would allow shorter extensions to be used, decreasing the likelihood of misfolding of the mutant RNA.

For the *RPS14A* pre-mRNA and mRNA used in our studies, the high affinity of PNA combined with the conformational sensitivity of the thiazole orange fluorogen allowed hybridization to occur and to be observed at low nanomolar PNA and RNA concentrations. While the ability of the PNA to report on its own hybridization (due to the enhanced TO fluorescence) is useful, the relatively low fluorescence quantum yield for TO ($\phi_f = 0.10-0.15$) leaves room for improvement, particularly in terms of a FRET donor. Dyes with higher quantum yields such as symmetrical cyanines (e.g., Cy3) (*40*) or Alexa dyes (*41*) could be substituted for TO without significantly affecting the hy-

bridization affinity for the RNA. Thus, TO-labeled PNA can be used to demonstrate hybridization, but switching to a different fluorophore can be used to optimize FRET efficiencies. Nevertheless, the studies reported here show that TO is sufficiently bright and photostable to be used under the demanding conditions of single-molecule measurements.

In a review of the FRET efficiency data for the different probe combinations, each set of probes gave the expected result of showing an increased FRET efficiency for spliced versus unspliced RNA. However, the **P1**−$\mathbf{10_A}$/**P2**−$\mathbf{13_{TO}}$ combination gave anomalously high FRET values for the unspliced RNA (Table 2). This result occurred in both bulk solution and single-molecule measurements. Meanwhile, using **P1**−$\mathbf{10_A}$ with a different donor (**P2**−$\mathbf{10_{TO}}$) or using **P2**−$\mathbf{13_{TO}}$ with a different acceptor (**P1**−$\mathbf{10_A}$) gives significantly lower FRET efficiencies for the unspliced RNA. Therefore, we cannot attribute the anomalous behavior to either probe. It is possible that the RNA adopts a different three-dimensional structure that brings the two probes into proximity when **P1**−$\mathbf{10_A}$ and **P2**−$\mathbf{13_{TO}}$ are used, although secondary structure prediction experiments do not show any significant differences (data not shown). Of the other three probe combinations, **P1**−$\mathbf{13_A}$/**P2**−$\mathbf{13_{TO}}$ is particularly effective, giving a 10−15-fold enhancement in FRET efficiency for the spliced RNA.

Finally, the results obtained here, particularly for **P1**−$\mathbf{13_A}$/**P2**−$\mathbf{13_{TO}}$, suggest that such probes can be used not only to label RNA and measure distances but also for real-time analysis. For example, splicing of the pre-mRNA should result in a large decrease in the TO fluorescence in conjunction with a large increase in the Alexa fluorescence. Such experiments will require that the hybridization probes not interfere with the spliceosome recognition and processing at the splice sites. Preliminary results indicate that this condition is met for the PNA probes and RNA substrate described here and will be reported fully in due course.

REFERENCES

1. Qin, P. Z., and Pyle, A. M. (1999) Site-Specific Labeling of RNA with Fluorophores and Other Structural Probes, *Methods 18*, 60−70.
2. Klostermeier, D., and Millar, D. P. (2001) RNA Conformation and Folding Studied with Fluorescence Resonance Energy Transfer, *Methods 23*, 240−254.
3. Ha, T. (2004) Structural Dynamics and Processing of Nucleic Acids Revealed by Single-Molecule Spectroscopy, *Biochemistry 43*, 4055−4063.
4. Li, N., Yu, C., and Huang, F. (2005) Novel Cyanine-AMP Conjugates for Efficient 5′-RNA Fluorescent Labeling by One-Step Transcription and Replacement of [γ-^{32}P]ATP in RNA Structural Investigation, *Nucleic Acids Res. 33*, e37.
5. Moore, M. J., and Query, C. C. (2000) Joining of RNAs by Splinted Ligation, *Methods Enzymol. 317*, 109−123.
6. Vaulèon, S., Ivanov, S. A., Gwiazda, S., and Müller, S. (2005) Site-Specific Fluorescent and Affinity Labeling of RNA by Using a Small Engineered Twin Ribozyme, *ChemBioChem 6*, 2158−2162.
7. Mergny, J.-L., Boutorine, A. S., Garestier, T., Belloc, F., Rougée, M., Bulychev, N. V., Koshkin, A. A., Bourson, J., Lebedev, A. V., Valeur, B., Thuong, N. T., and Hélène, C. (1994) Fluorescence Energy Transfer as a Probe for Nucleic Acid Structures and Sequences, *Nucleic Acids Res. 22*, 920−928.
8. Okamura, Y., Kondo, S., Sase, I., Suga, T., Mise, K., Furusawa, I., Kawakami, S., and Watanabe, Y. (2000) Double-Labeled Donor Probe Can Enhance the Signal of Fluorescence Resonance Energy Transfer (FRET) in Detection of Nucleic Acid Hybridization, *Nucleic Acids Res. 28*, e107.
9. Sei-lida, Y., Koshimoto, H., Kondo, S., and Tsuji, A. (2000) Real-Time Monitoring of In Vitro Transcriptional RNA Synthesis Using Fluorescence Resonance Energy Transfer, *Nucleic Acids Res. 28*, e59.
10. Tsuji, A., Koshimoto, H., Sato, Y., Hirano, M., Sei-lida, Y., Kondo, S., and Ishibashi, K. (2000) Direct Observation of Specific Messenger RNA in a Single Living Cell Under a Fluorescence Microscope, *Biophys. J. 78*, 3260−3274.
11. Tsuji, A., Sato, Y., Hirano, M., Suga, T., Koshimoto, H., Taguchi, T., and Ohsuka, S. (2001) Development of a Time-Resolved Fluorometric Method for Observing Hybridization in Living Cells Using Fluorescence Resonance Energy Transfer, *Biophys. J. 81*, 501−515.
12. Dorywalska, M., Blanchard, S. C., Gonzalez, R. L., Jr., Kim, H. D., Chu, S., and Puglisi, J. D. (2005) Site-Specific Labeling of the Ribosome for Single-Molecule Spectroscopy, *Nucleic Acids Res. 33*, 182−189.
13. Smith, G. J., Sosnick, T. R., Scherer, N. F., and Pan, T. (2005) Efficient Fluorescence Labeling of a Large RNA Through Oligonucleotide Hybridization, *RNA 11*, 234−239.
14. Clegg, R. M. (1995) Fluorescence Resonance Energy Transfer, *Curr. Opin. Biotechnol. 6*, 103−110.
15. Nielsen, P. E., Egholm, M., Berg, R. H., and Buchardt, O. (1991) Sequence-Selective Recognition of DNA by Strand Displacement with a Thymine-Substituted Polyamide, *Science 254*, 1498−1500.
16. Nielsen, P. E., and Egholm, M. (2004) in *Peptide Nucleic Acids: Protocols and Applications* (Nielsen, P. E., Ed.) 2nd ed., pp 1−36, Horizon Bioscience, Norfolk, U.K.
17. Egholm, M., Buchardt, O., Christensen, L., Behrens, C., Freier, S. M., Driver, D. A., Berg, R. H., Kim, S. K., Nordén, B., and Nielsen, P. E. (1993) PNA Hybridizes to Complementary Oligonucleotides Obeying the Watson−Crick Hydrogen-Bonding Rules, *Nature 365*, 566−568.
18. Hanvey, J. C., Peffer, N. J., Bisi, J. E., Thomson, S. A., Cadilla, R., Josey, J. A., Ricca, D. J., Hassman, C. F., Bonham, M. A., Au, K. G., Carter, S. G., Bruckenstein, D. A., Boyd, A. L., Noble, S. A., and Babiss, L. E. (1992) Antisense and Antigene Properties of Peptide Nucleic Acids, *Science 258*, 1481−1485.
19. Knudsen, H., and Nielsen, P. E. (1996) Antisense Properties of Duplex- and Triplex-Forming PNAs, *Nucleic Acids Res. 24*, 494−500.
20. Karadag, A., Riminucci, M., Bianco, P., Cherman, N., Kuznetsov, S. A., Nguyen, N., Collins, M. T., Robey, P. G., Fisher, L. W. (2004) A Novel Technique Based on a PNA Hybridization Probe and FRET Principle for Quantification of Mutant Genotype in Fibrous Dysplasia/McCune-Albright Syndrome, *Nucleic Acids Res. 32*, e63.
21. Zhuang, X. (2005) Single-Molecule RNA Science, *Annu. Rev. Biophys. Biomol. Struct. 34*, 399−414.
22. Zhou, X.-f., Peng, Z.-h., Geise, J., Peng, B.-x., Li, Z.-x., Yan, M., Domisse, R., Carieer, R., and Claeys, M. (1995) Blue Sensitizing Dyes: Synthesis, Spectroscopy, and Performance in Photographic Emulsions, *J. Imaging Sci. Technol. 39*, 244−252.
23. Svanvik, N., Westman, G., Wang, D., and Kubista, M. (2000) Light-Up Probes: Thiazole Orange-Conjugated Peptide Nucleic Acid for Detection of Target Nucleic Acid in Homogeneous Solution, *Anal. Biochem. 281*, 26−35.
24. Christensen, L., Fitzpatrick, R., Gildea, B., Petersen, K. H., Hansen, H. F., Koch, T., Egholm, M., Buchardt, O., Nielsen, P. E., Coull, J., and Berg, R. H. (1995) Solid-Phase Synthesis of Peptide Nucleic Acids, *J. Pept. Sci. 3*, 175−183.
25. Koch, T. (2004) in *Peptide Nucleic Acids: Protocols and Applications* (Nielsen, P. E., Ed.) 2nd ed., pp 37−60, Horizon Bioscience, Norfolk, U.K.
26. Kubin, R. F., and Fletcher, A. N. (1982) Fluorescence Quantum Yields of Some Rhodamine Dyes, *J. Lumin. 27*, 455−462.
27. Dhami, S., de Mello, A. J., Rumbles, G., Bishop, S. M., Phillips, D., and Beeby, A. (1995) Phthalocyanine Fluorescence at High Concentration: Dimers or Reabsorption Effect? *Photochem. Photobiol. 61*, 341.
28. Williams, A. T. R., Winfield, S. A., and Miller, J. N. (1983) Relative Fluorescence Quantum Yield Using a Computer Controlled Luminescence Spectrometer, *Analyst 108*, 1067.
29. Ha, T. (2001) Single-Molecule Fluorescence Resonance Energy Transfer, *Methods 25*, 78−86.
30. Hamilton, S. E., Pitts, A. E., Katipally, R. R., Jia, X., Rutter, J. P., Davies, B. A., Shay, J. W., Wright, W. E., and Corey, D. R. (1997) Identification of Determinants for Inhibitor Binding within

the Active Site of Human Telomerase Using PNA Scanning, *Biochemistry 36*, 11873−11880.
31. Nygren, J., Svanvik, N., and Kubista, M. (1998) The Interactions Between the Fluorescent Dye Thiazole Orange and DNA, *Biopolymers 46*, 39−51.
32. Lee, L. G., Chen, C., and Liu, L. A. (1986) Thiazole Orange: A New Dye for Reticulocyte Analysis, *Cytometry 7*, 508−517.
33. Wittung, P., Kim, S. K., Buchardt, O., Nielsen, P. E., and Nordèn, B. (1994) Interactions of DNA Binding Ligands with PNA-DNA Hybrids, *Nucleic Acids Res. 22*, 5371−5377.
34. Ishiguro, T., Saitoh, J., Yawata, H., Otsuka, M., Inoue, T., and Sugiura, Y. (1996) Fluorescence Detection of Specific Sequence of Nucleic Acids by Oxazole Yellow-Linked Oligonucleotides. Homogeneous Quantitative Monitoring of *In Vivo* Transcription, *Nucleic Acids Res. 24*, 4992−4997.
35. Isacsson, J., Cao, H., Ohlsson, L., Nordgren, S., Svanvik, N., Westman, G., Kubista, M., Sjøback, R., and Sehlstedt, U. (2000) Rapid and Specific Detection of PCR Products Using Light-Up Probes, *Mol. Cell. Probes 14*, 321−328.
36. Köhler, O., Jarikote, D. V., and Seitz, O. (2005) Forced Intercalation Probes (FIT Probes): Thiazole Orange as a Fluorescent Base in Peptide Nucleic Acids for Homogeneous Single-Nucleotide-Polymorphism Detection, *ChemBioChem 6*, 69−77.
37. Marin, V. L., and Armitage, B. A. (2005) RNA Guanine Quadruplex Invasion by Complementary and Homologous PNA Probes, *J. Am. Chem. Soc. 127*, 8032−8033.
38. Marin, V. L., and Armitage, B. A. (2006) Hybridization of Complementary and Homologous Peptide Nucleic Acid Oligomers to a Guanine Quadruplex-Forming RNA, *Biochemistry 45*, 1745−1754.
39. Svanvik, N., Nygren, J., Westman, G., and Kubista, M. (2001) Free-Probe Fluorescence of Light-Up Probes, *J. Am. Chem. Soc. 123*, 803−809.
40. Mujumdar, R. B., Ernst, L. A., Mujumdar, S. R., Lewis, C. J., and Waggoner, A. S. (1993) Cyanine Dye Labeling Reagents: Sulfoindocyanine Succinimidyl Esters, *Bioconjugate Chem. 4*, 105−111.
41. Panchuk-Voloshina, N., Haugland, R. P., Bishop-Stewart, J., Bhalgat, M. K., Millard, P. J., Mao, F., Leung, W.-Y., and Haugland, R. P. (1999) Alexa Dyes, a Series of New Fluorescent Dyes that Yield Exceptionally Bright, Photostable Conjugates, *J. Histochem. Cytochem. 47*, 1179−1188.

BI052050S